

# Radar Target Recognition by Frequency-Diversity RCS Together with Kernel Scatter Difference Discrimination

Kun-Chou Lee\*

**Abstract**—In this paper, the radar target recognition is given by frequency-diversity RCS (radar cross section) together with kernel scatter difference discrimination. The frequency-diversity technique means to collect electromagnetic signals by sweeping the operation frequencies. Such a technique is usually utilized in inverse scattering and radar target recognition because different frequencies each may contain important information of a target. By using the frequency diversity RCS technique, one can reduce the times of spatial measurement. This is an important contribution since it is always difficult to build a spatial radar measurement in practical battlefield environments. To enhance pattern recognition, the collected RCS data are processed by the kernel scatter difference discrimination, which is improved from the Fisher discrimination. To investigate the capability of tolerating environmental fluctuation, each simulated RCS data is added by a random component prior to implementing pattern recognition. Numerical simulation shows that our recognition scheme is still very accurate even though the RCS contains a random component.

## 1. INTRODUCTION

The efficiency of a weapon system directly depends on the target recognition capability of a radar system in modern battlefield environments [1]. Traditional radar identification technology usually utilizes a target's images for identification, e.g., SAR (synthetic aperture radar) [2, 3] and ISAR (inverse synthetic aperture radar) [4, 5]. Although these techniques work well, radar images are difficult to obtain due to the expensive hardware. In general, measuring RCS (radar cross section) [6, 7] is easier than achieving radar images. This motivates us to implement target recognition through RCS. The RCS is affected by frequencies, spatial directions and polarizations. Target recognition by original RCS usually involves enormous data computations. To achieve efficient and reliable recognition, the original RCS data are often projected to an eigenspace prior to identification. The goal is to reduce the data complexity and enhance the discrimination.

Practically, the techniques of collecting electromagnetic signals for inverse scattering are divided into three categories, which are angular, frequency and polarization diversities [8, 9]. Among these three techniques, the frequency diversity [10, 11] is the most efficient so that it becomes very important in inverse scattering. Such a diversity technique means to collect electromagnetic signals by sweeping the operation frequencies. In general, a target always contains special information at different frequencies. Physically, the radar target recognition is a simple and rough approach of inverse scattering. Therefore, it is reasonable to expect that the frequency diversity technique is also useful in RCS based target recognition. Compared with angular-diversity RCS (i.e., collecting electromagnetic signals by changing spatial angles) [12–14], the frequency-diversity RCS technique is more efficient and contains much more

---

*Received 12 October 2019, Accepted 2 December 2019, Scheduled 16 December 2019*

\* Corresponding author: Kun-Chou Lee (kclee@mail.ncku.edu.tw).

The author is with the Department of Systems and Naval Mechatronic Engineering, National Cheng-Kung University, Tainan 701, Taiwan.

information for identification. This then motivates us to implement radar target recognition by using frequency-diversity RCS.

In this paper, the radar target recognition is given by frequency-diversity RCS together with kernel scatter difference discrimination [14–16]. The kernel scatter difference discrimination [14–16] improves conventional Fisher discrimination [17] in computational efficiency, but is not affected by the matrix singularity. Such a pattern recognition technique is based on the differences between “kernel between-class” and “kernel within-class” matrices of scatters. The “kernel between-class” scatter matrix represents the mean distance between centers of different classes in eigenspace, and is expected to be as large as possible. Whereas the “kernel within-class” scatter matrix represents the mean distance between samples within the same class and their center, and is expected to be as small as possible. Thus one can calculate the eigenvalues and eigenvectors in eigenspace. Initially, the frequency-diversity RCS data are collected and projected to the eigenspace. Next, eigenvectors corresponding to several largest eigenvalues are selected as the principal components in eigenspace. Finally, the Euclidean distance in eigenspace is calculated for identifying types of targets. Numerical simulation shows that our radar target recognition scheme can identify targets accurately and efficiently, even though there exist random noises.

In the following, theoretical formulations are given in Section 2. Numerical simulation results are given in Section 3. Finally, conclusions are given in Section 4.

## 2. FORMULATIONS

This study has no limitation on the types of targets. With loss of generality, we utilize the ship model as the target for simplicity. Consider a ship on the sea level ( $X$ - $Y$  plane), as shown in Fig. 1. The front end and broadside of a ship are in directions of  $+X$  and  $\pm Y$ , respectively. A spatial location is characterized by spherical coordinates  $(R, \theta, \phi)$ , where  $R$  is the distance to the coordinate origin,  $\theta$  the elevation angle, and  $\phi$  the azimuth angle. The ship is illuminated by a horizontally propagating plane wave  $\bar{E}_i$  with  $\hat{z}$ -polarization and unit magnitude. This incident wave will produce a scattered electric field and then the RCS. The RCS means the relative power magnitude of the reflected electromagnetic signals from a target. Mathematically, the bistatic RCS in the direction of  $(\theta, \phi)$  is defined as [6]

$$\text{RCS}(\theta, \phi) = \lim_{R \rightarrow \infty} 4\pi R^2 \frac{|\bar{E}_S(\theta, \phi)|^2}{|\bar{E}_i|^2} \quad (1)$$

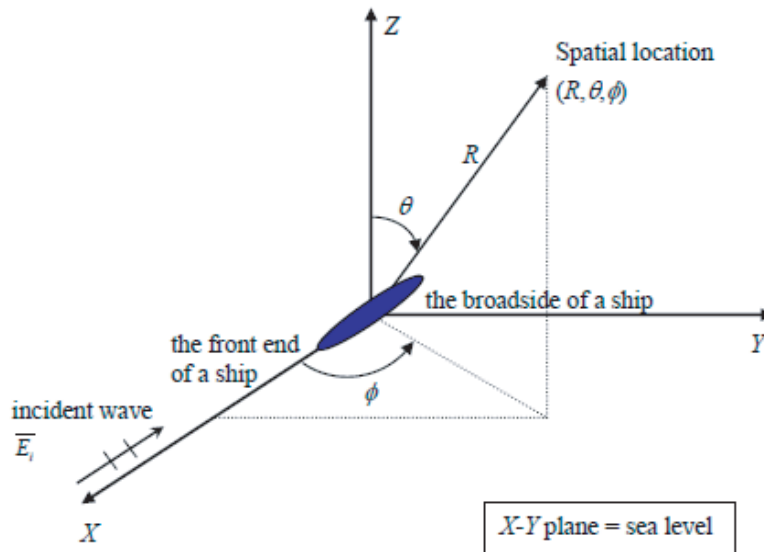


**Figure 1.** Schematic diagram of a ship illuminated by an incident plane wave.

where  $\bar{E}_i$  is the incident electric field, and  $\bar{E}_S(\theta, \phi)$  is the scattered electric field. As mentioned above, a target always contains special information at different frequencies. Therefore, this study utilizes frequency-diversity technique to collect RCS data for target identification.

Our recognition scheme includes two stages, which are training and testing. In the training stage, we first select training vectors. Assume there are  $P$  ( $p = 1, \dots, P$ ) categories of known ships. For each ship in Fig. 1, the incident wave horizontally propagates toward the target from the azimuth angles of  $\phi_i = 0^\circ, 90^\circ$  and  $180^\circ$ , sequentially. For each incident azimuth angle ( $\phi_i$ ), the RCS data are collected in the direction of  $(\theta, \phi_i)$  where  $\theta$  is changed as  $\theta_1, \theta_2, \dots$ , and  $\theta_N$ , sequentially. For each direction, the operation frequency is swept as  $f_1, f_2, \dots$ , and  $f_M$ , sequentially. Thus we have a frequency-diversity signal matrix with the dimension of  $(3M) \times (NP)$ , as shown in Fig. 2.

		category #1 fishing boat				category #2 naval ship				category #3 container vessel			
		$\theta_1$	$\theta_2$	$\dots$	$\theta_N$	$\theta_1$	$\theta_2$	$\dots$	$\theta_N$	$\theta_1$	$\theta_2$	$\dots$	$\theta_N$
$\phi_i = 0^\circ$	$f_1$	RCS	RCS	$\dots$	RCS	RCS	RCS	$\dots$	RCS	RCS	RCS	$\dots$	RCS
	$f_2$	RCS	RCS	$\dots$	RCS	RCS	RCS	$\dots$	RCS	RCS	RCS	$\dots$	RCS
	$\vdots$	$\vdots$	$\vdots$	$\dots$	$\vdots$	$\vdots$	$\vdots$	$\dots$	$\vdots$	$\vdots$	$\vdots$	$\dots$	$\vdots$
	$f_M$	RCS	RCS	$\dots$	RCS	RCS	RCS	$\dots$	RCS	RCS	RCS	$\dots$	RCS
$\phi_i = 90^\circ$	$f_1$	RCS	RCS	$\dots$	RCS	RCS	RCS	$\dots$	RCS	RCS	RCS	$\dots$	RCS
	$f_2$	RCS	RCS	$\dots$	RCS	RCS	RCS	$\dots$	RCS	RCS	RCS	$\dots$	RCS
	$\vdots$	$\vdots$	$\vdots$	$\dots$	$\vdots$	$\vdots$	$\vdots$	$\dots$	$\vdots$	$\vdots$	$\vdots$	$\dots$	$\vdots$
	$f_M$	RCS	RCS	$\dots$	RCS	RCS	RCS	$\dots$	RCS	RCS	RCS	$\dots$	RCS
$\phi_i = 180^\circ$	$f_1$	RCS	RCS	$\dots$	RCS	RCS	RCS	$\dots$	RCS	RCS	RCS	$\dots$	RCS
	$f_2$	RCS	RCS	$\dots$	RCS	RCS	RCS	$\dots$	RCS	RCS	RCS	$\dots$	RCS
	$\vdots$	$\vdots$	$\vdots$	$\dots$	$\vdots$	$\vdots$	$\vdots$	$\dots$	$\vdots$	$\vdots$	$\vdots$	$\dots$	$\vdots$
	$f_M$	RCS	RCS	$\dots$	RCS	RCS	RCS	$\dots$	RCS	RCS	RCS	$\dots$	RCS

Figure 2. Illustration of the frequency-diversity signal matrix.

This study utilizes the kernel scatter difference discrimination [14–16] for identification. The details of kernel scatter difference discrimination can be found in References [14–16]. The pattern recognition procedures are briefly given in the following. Assume  $\bar{x}_i^p$  denotes the  $i$ -th column in category # $p$  of Fig. 2. It is a training vector in the original RCS data space. In the kernel scatter difference discrimination [14–16],  $\bar{x}_i^p$  is projected to a higher dimensional feature space  $F$  through a mapping function  $\bar{\Phi}(\cdot)$  as

$$\bar{x}_i^p \rightarrow \bar{\Phi}(\bar{x}_i^p) \in F, \quad p = 1, 2, \dots, P; \quad i = 1, 2, \dots, N. \tag{2}$$

In the kernel mapping, the “kernel between-class” scatter matrix  $\bar{\bar{K}}_B$  and “kernel within-class” scatter matrix  $\bar{\bar{K}}_W$  are defined as [14–16]

$$\bar{\bar{K}}_B = \sum_{p=1}^P (\bar{u}_p - \bar{u}_{\text{mean}}) \cdot (\bar{u}_p - \bar{u}_{\text{mean}})^T \tag{3}$$

and

$$\overline{\overline{K}}_W = \frac{1}{N} \sum_{p=1}^P \sum_{i=1}^N (\overline{\delta}_i^p - \overline{u}_p) \cdot (\overline{\delta}_i^p - \overline{u}_p)^T \quad (4)$$

where

$$\overline{u}_p = \frac{1}{N} \left( \sum_{i=1}^N \kappa(\overline{x}_1^1, \overline{x}_i^p), \dots, \sum_{i=1}^N \kappa(\overline{x}_N^1, \overline{x}_i^p), \dots, \sum_{i=1}^N \kappa(\overline{x}_1^P, \overline{x}_i^p), \dots, \sum_{i=1}^N \kappa(\overline{x}_N^P, \overline{x}_i^p) \right)^T \quad (5)$$

$$\overline{\delta}_i^p = (\kappa(\overline{x}_1^1, \overline{x}_i^p), \dots, \kappa(\overline{x}_N^1, \overline{x}_i^p), \dots, \kappa(\overline{x}_1^P, \overline{x}_i^p), \dots, \kappa(\overline{x}_N^P, \overline{x}_i^p))^T \quad (6)$$

and

$$\overline{u}_{\text{mean}} = \frac{1}{N \cdot P} \sum_{p=1}^P \sum_{i=1}^N \overline{\delta}_i^p. \quad (7)$$

The symbol “ $T$ ” in Eqs. (3)–(6) denotes the transposition. The notation  $\kappa(\cdot)$  in Eqs. (5)–(6) is a kernel transformation, which is defined as

$$\kappa(\overline{x}, \overline{y}) = (\overline{x} \cdot \overline{y})^d \quad (8)$$

where  $d$  is the kernel polynomial degree [14–16]. The scatter-difference based discrimination function is given as [14–16]

$$J(\overline{\varepsilon}) = \left| \overline{\varepsilon}^T \left( \overline{\overline{K}}_B - \ell \cdot \overline{\overline{K}}_W \right) \overline{\varepsilon} \right| \quad (9)$$

where  $\overline{\varepsilon}$  is the optimal transformation matrix, and  $\ell$  is the impact parameter. By adjusting the impact parameter  $\ell$  in Eq. (9), one can control the impact from  $\overline{\overline{K}}_B$  or  $\overline{\overline{K}}_W$ . The optimal transformation matrix in Eq. (9) is given as  $\overline{\varepsilon} = (\overline{w}_1, \overline{w}_2, \dots, \overline{w}_e)$  where  $\overline{w}_1, \overline{w}_2, \dots$ , and  $\overline{w}_e$  are principal eigenvectors. These principal eigenvectors will be introduced later. As all training vectors are mapped via the optimal transformation matrix  $\overline{\varepsilon}$ , the discrimination function  $J(\overline{w}_i)$  in Eq. (9) will be maximized. That is, the “kernel between-class” scatter matrix  $\overline{\overline{K}}_B$  is maximized and the “kernel within-class” scatter matrix  $\overline{\overline{K}}_W$  is minimized. This is the optimal discrimination and then the goal of pattern recognition.

Each principal eigenvector is normalized as  $\|\overline{w}_i\| = 1$ ,  $i = 1, 2, \dots, e$ . Thus maximizing  $J(\overline{w}_i)$  is equivalent to finding the maximum of the Lagrange function  $L(\overline{w}_i, \lambda)$  [14–16] where

$$L(\overline{w}_i, \lambda) = J(\overline{w}_i) - \lambda (\|\overline{w}_i\| - 1), \quad i = 1, 2, \dots, e. \quad (10)$$

By taking the partial differential of the above function with respect to  $\overline{w}_i$  and setting the result to be zero, we have

$$\left( \overline{\overline{K}}_B - \ell \cdot \overline{\overline{K}}_W \right) \overline{w}_i = \lambda \overline{w}_i. \quad (11)$$

There are  $NP$  eigenvalues (i.e., solutions of  $\lambda$ ) in Eq. (11) and these eigenvalues are ranked as  $\lambda_1 \geq \lambda_2 \geq \dots \geq \lambda_{NP}$ . We select the top  $e$  ( $e < NP$ ) eigenvalues ( $\lambda_1 \geq \lambda_2 \geq \dots \geq \lambda_e$ ) and their corresponding eigenvectors  $\overline{w}_1, \overline{w}_2, \dots, \overline{w}_e$  as principal components for eigenspace of kernel scatter difference. That is, principal eigenvectors  $\overline{w}_1, \overline{w}_2, \dots, \overline{w}_e$  will span the eigenspace of kernel scatter difference.

After constructing the eigenspace through the principal eigenvectors, one can project an arbitrary signal vector  $\overline{x}$  to a higher dimensional space and then to the eigenspace. The resulting feature vector is

$$\overline{\Omega} = (\overline{w}_1, \overline{w}_2, \dots, \overline{w}_e)^T \cdot (\kappa(\overline{x}_1^1, \overline{x}), \dots, \kappa(\overline{x}_N^1, \overline{x}), \dots, \kappa(\overline{x}_1^P, \overline{x}), \dots, \kappa(\overline{x}_N^P, \overline{x})). \quad (12)$$

All training vectors are projected to the eigenspace by Eq. (12). The center or mean of feature vectors for each category in eigenspace is calculated as

$$\overline{\Omega}_{\text{mean}}^p = \frac{1}{N} \sum_{i=1+N(p-1)}^{N \cdot p} \overline{\Omega}_i, \quad p = 1, 2, \dots, P. \quad (13)$$

In the testing stage, the RCS vector  $\bar{x}$  of an unknown target is collected, mapped to the feature space  $F$ , and then projected to the eigenspace by Eq. (12). Thus, an  $e$ -dimensional feature vector  $\bar{\Omega}$  as Eq. (12) is obtained. Finally, the Euclidean distance from the testing vector to the center of each category in eigenspace is calculated as

$$\Gamma_p = \|\bar{\Omega} - \bar{\Omega}_{\text{mean}}^p\|, \quad p = 1, 2, \dots, P. \quad (14)$$

One can use the Euclidean distance of Eq. (14) to estimate the similarity between the unknown and known targets. If the testing vector is the closest (i.e., with the smallest Euclidean distance) to the  $p$ -th category, we judge the unknown target to be a ship of the  $p$ -th category.

### 3. NUMERICAL SIMULATION RESULTS

In this section, numerical examples are given to verify the above formulations. For simplicity, models of ships are considered as targets instead of real ships. As illustrated in Fig. 3, there are three categories of ships ( $P = 3$ ) for modeling the fishing boat (category #1), naval ship (category #2) and container vessel (category #3). The ship size is  $kr_1 = 3.1$  for category #1,  $kr_2 = 6.3$  for category #2, and  $kr_3 = 9.4$  for category #3, where  $k$  is the wavenumber, and  $r_p$  ( $p = 1, 2, 3$ ) represents the length of a ship. All ships are assumed to be on the sea level ( $X$ - $Y$  plane) and the characteristic for surface roughness of sea water is assumed to be

$$z(x, y) = \frac{4}{75}r_p \cdot \sin\left(\frac{15}{4}\pi x\right) \sin\left(\frac{15}{4}\pi y\right) + \frac{8}{75}r_p. \quad (15)$$

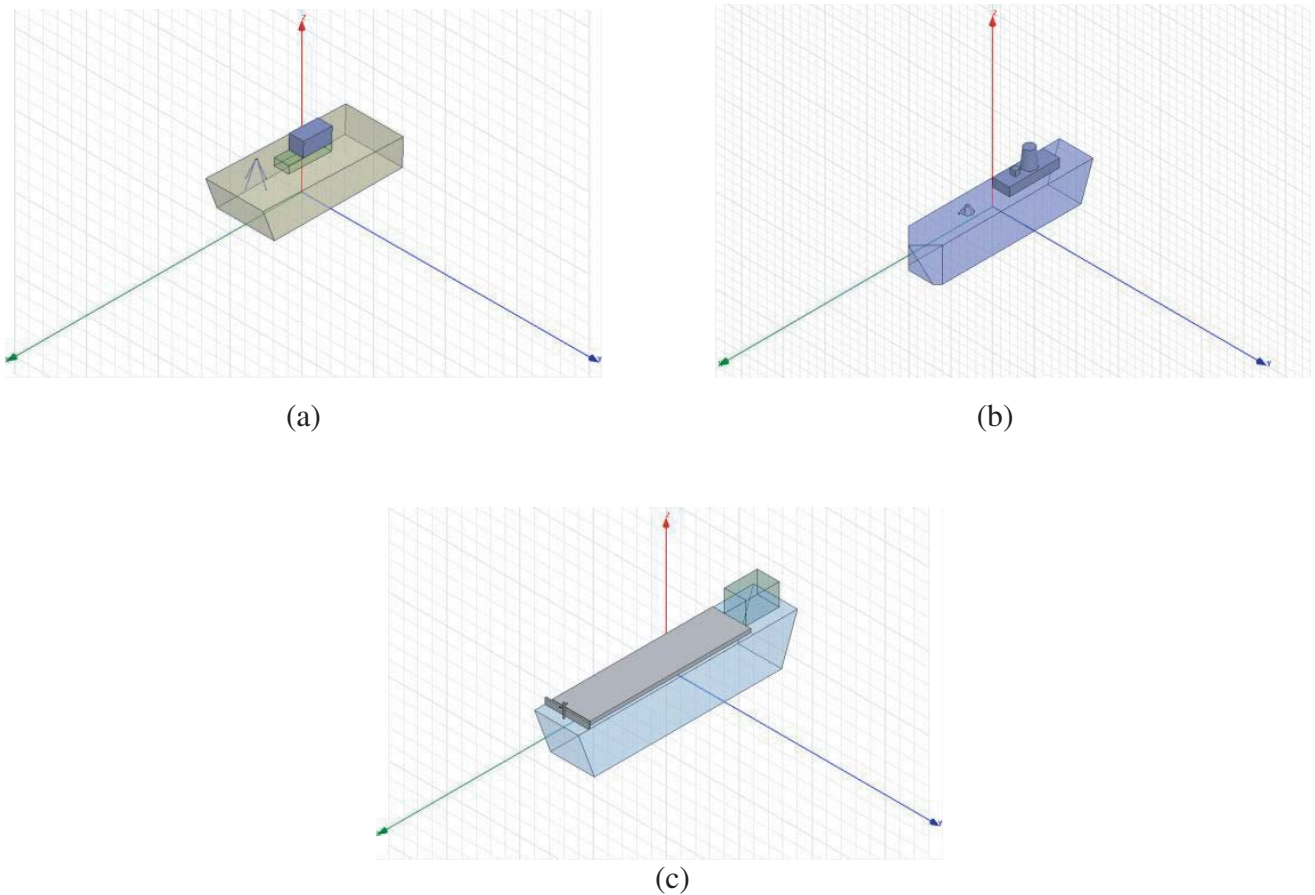


**Figure 3.** Geometrical structures for the three categories of known ships: (a) category #1, (b) category #2 and (c) category #3.

The sea water has a dielectric constant  $\varepsilon_r = 81$  and conductivity  $\sigma = 4 \text{ S/m}$ . In numerical simulation, we utilize the Ansys HFSS (High Frequency Structure Simulator) software to calculate the RCS of ships.

In the training stage, the frequency-diversity signal matrix is first constructed. For each incident azimuth angle ( $\phi_i = 0^\circ$  or  $90^\circ$  or  $180^\circ$ ), the RCS data are collected in the direction of  $(\theta, \phi_i)$  where  $\theta$  is changed as  $\theta_1 = 61^\circ$ ,  $\theta_2 = 63^\circ$ , ..., and  $\theta_{15} = 89^\circ$ , sequentially. For each direction, the operation frequency is swept as  $f_1 = 3.1 \text{ GHz}$ ,  $f_2 = 3.2 \text{ GHz}$ , ..., and  $f_{10} = 3.9 \text{ GHz}$ . Thus we have a frequency-diversity signal matrix with the dimension of  $30 \times 45$ , as shown in Fig. 2.

In the testing stage, the arrangement for collecting the RCS of an unknown ship is the same as that of the training stage, except that the evaluation angles are changed as  $\theta_1 = 62^\circ$ ,  $\theta_2 = 64^\circ$ , ..., and  $\theta_{15} = 90^\circ$ . Note that the evaluation angles of the testing stage are different from those of the training stage. Such an arrangement is for investigating the ability to identify examples that have not been learned. Our goal is to identify which training (known) ship is the most similar to the testing (unknown) ship by using Eq. (14). In our treatment, the number of principal components ( $e$ ) and the kernel polynomial degree ( $d$ ) are set to be  $e = d = 1$  based on research experiences.

In the first example, we choose the ship of category #1 (i.e., a fishing boat) as the tested (unknown) target. Following the procedures of Section 2, the distance to feature's center of each category is calculated by Eq. (14) and then given in Fig. 4. From Fig. 4, it is shown that the line of  $\Gamma_1$  is the lowest for each testing elevation angle  $\theta$ . Thus we judge the unknown target to be a fishing boat (i.e., category #1 of known ships). This recognition result is consistent with the fact. The judgments are all correct for all the 15 testing elevation angles. The correct recognition rate is 100% (15/15).

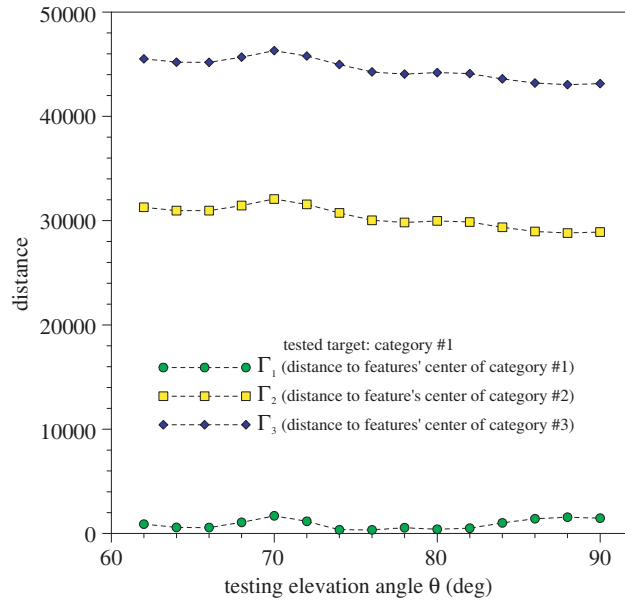


**Figure 4.** The distance to feature's center of each category by using the ship of category #1 (i.e., a fishing boat) as the tested target.

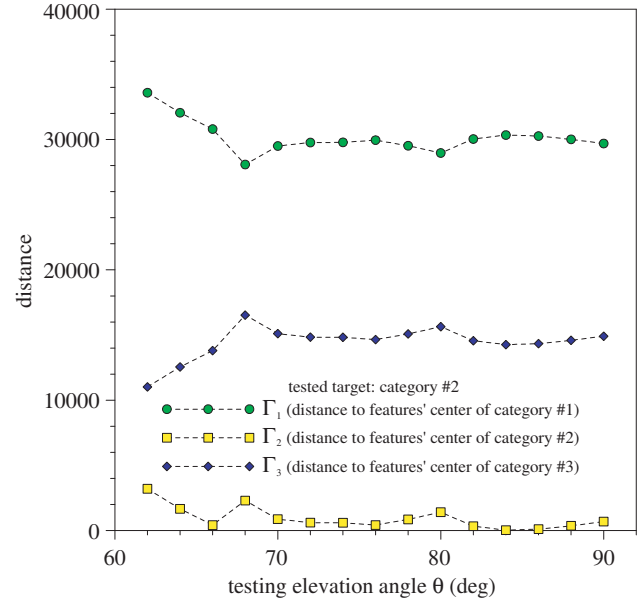


**Figure 5.** The distance to feature's center of each category by using the ship of category #2 (i.e., a naval ship) as the tested target.

In the second example, we choose the ship of category #2 (i.e., a naval ship) as the tested (unknown) target. The other arrangements are the same as those of the first example. The distance to feature's center of each category is calculated by Eq. (14) and then given in Fig. 5. Fig. 5 shows that the line of  $\Gamma_2$  is the lowest for each testing elevation angle  $\theta$ . Thus we judge the unknown target to be a naval ship (i.e., category #2 of known ships). This recognition result is consistent with the fact. The judgments are all correct for all the 15 testing elevation angles. The correct recognition rate is 100% (15/15).

In the third example, we choose the ship of category #3 (i.e., a container vessel) as the tested (unknown) target. The other arrangements are the same as the previous two examples. The distance to feature's center of each category is calculated by Eq. (14) and then given in Fig. 6. From Fig. 6, it reports

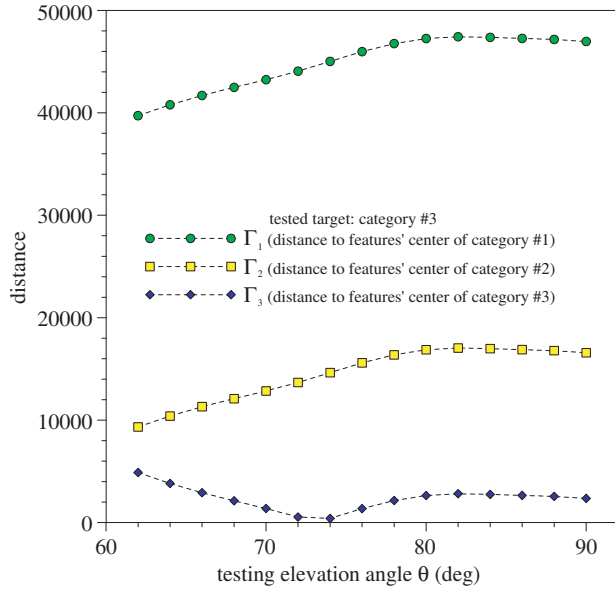


**Figure 6.** The distance to feature’s center of each category by using the ship of category #3 (i.e., a container vessel) as the tested target.

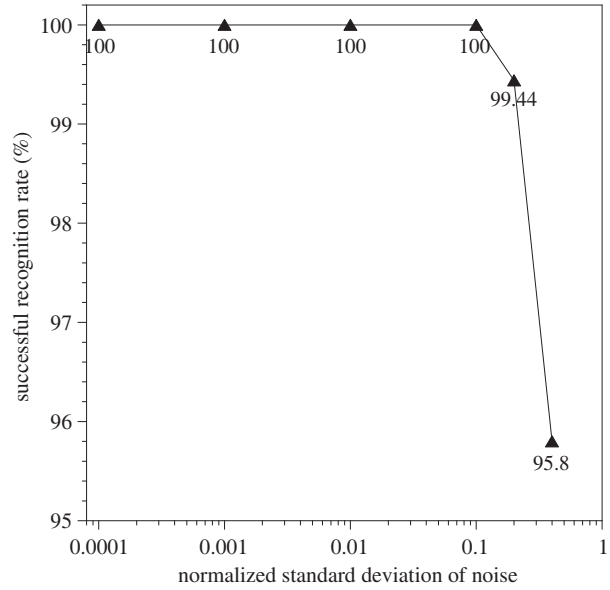


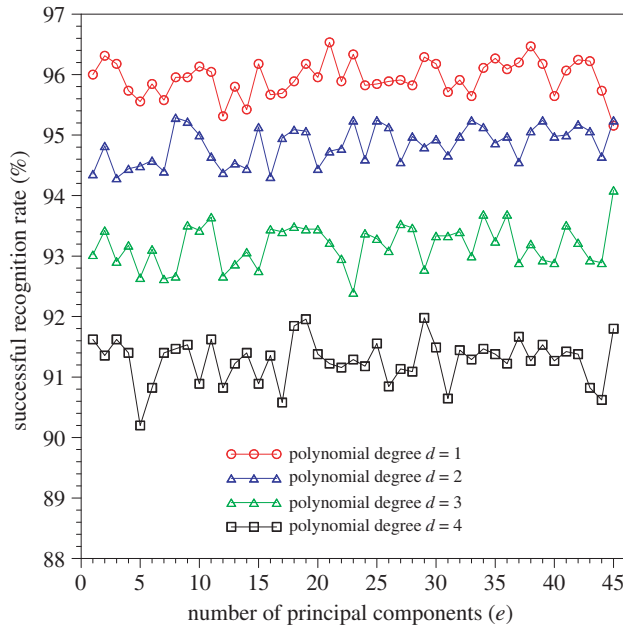
**Figure 7.** The successful recognition rate with respect to different levels of random noises.

that the line of  $\Gamma_3$  is the lowest for each testing elevation angle  $\theta$ . Thus we judge the unknown target to be a container vessel (i.e., category #3 of known ships). The recognition result is consistent with the fact. The judgments are all correct for all the 15 testing elevation angles. The correct recognition rate is 100% (15/15). From the above three examples, the overall successful recognition rate is 100% (45/45).

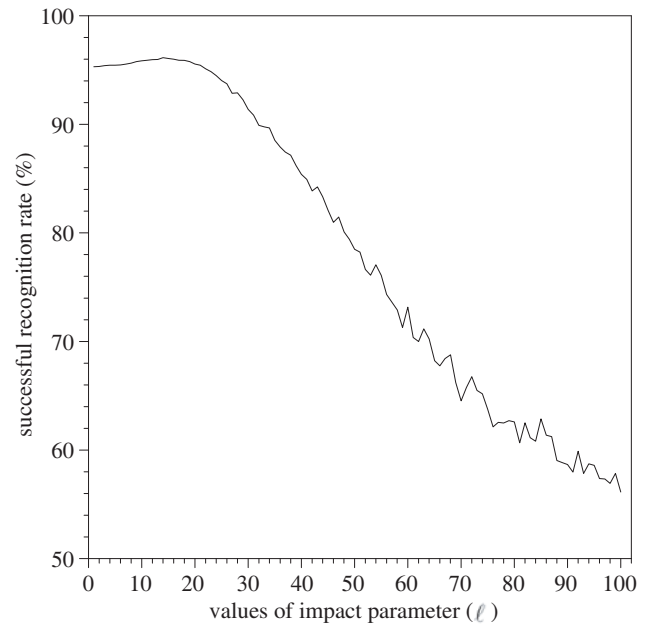
To understand whether the proposed recognition scheme is affected by noises, we add a random component to each computed RCS. The random component is generated by Gaussian distribution with zero-mean. The standard deviation of noise distribution is normalized by the root-mean-square RCS and is chosen as  $10^{-4}$ ,  $10^{-3}$ ,  $10^{-2}$ ,  $10^{-1}$ ,  $2 \times 10^{-1}$ , and  $4 \times 10^{-1}$ , respectively. Fig. 7 shows the successful recognition rate with respect to different levels of random noises for our recognition scheme. The noise level here means the normalized standard deviation of random components. From Fig. 7, it shows that the successful recognition rate is 100%, 100%, 100%, 100%, 99.44%, and 95.8%, for noise levels of  $10^{-4}$ ,  $10^{-3}$ ,  $10^{-2}$ ,  $10^{-1}$ ,  $2 \times 10^{-1}$ , and  $4 \times 10^{-1}$ , respectively. Fig. 7 reports that the successful recognition rate is still greater than 95%, even though the noise level is increased to  $4 \times 10^{-1}$ . This implies that the proposed recognition scheme has very good ability to tolerate random noises.

Figure 8 shows the successful recognition rate with respect to the number of principal components ( $e$ ) under different choices of kernel polynomial degree ( $d$ ). In Fig. 8, the noise level is set as  $4 \times 10^{-1}$ , i.e., the worst case of noise effects. Fig. 8 reports that the recognition rate is always greater than 90% for all choices of principal components ( $e$ ) and kernel polynomial degree ( $d$ ). This implies that the kernel scatter difference discrimination is a very good pattern recognition technique in such a problem. Fig. 8 also reports that the kernel polynomial degree ( $d$ ) is an important factor in our recognition scheme, whereas the impact from the number of principal components ( $e$ ) is not significant.

In Eq. (9), the scatter-difference based discrimination function is affected by the kernel between-class scatter matrix  $\overline{\overline{K}}_B$  and kernel within-class scatter matrix  $\overline{\overline{K}}_W$ . The weight of impact from  $\overline{\overline{K}}_B$  and  $\overline{\overline{K}}_W$  are controlled by adjusting the impact parameter ( $\ell$ ). Fig. 9 shows the successful recognition rate with respect to different values of impact parameter ( $\ell$ ). Similar to Fig. 8, the noise level of Fig. 9 is set as  $4 \times 10^{-1}$ , which is the worst case of noise effects. From Fig. 9, it reports that successful recognition rate is generally in negative correlation with the impact parameter ( $\ell$ ), and has the maximum at  $\ell = 14$ . Thus  $\ell = 14$  is the best choice in this study. Therefore, we choose  $\ell = 14$  as the impact parameter in the above three numerical examples.



**Figure 8.** The successful recognition rate with respect to the number of principal components ( $e$ ) under different choices of kernel polynomial degree ( $d$ ).



**Figure 9.** The successful recognition rate with respect to different values of impact parameter ( $\ell$ ).

#### 4. CONCLUSIONS

In this paper, the radar target recognition is successfully implemented by frequency-diversity RCS together with kernel scatter difference discrimination. The frequency-diversity RCS technique of this study required  $3 \times 15 = 45$  spatial directions (i.e., 3 azimuth angles and 15 elevation angles) in constructing the signal matrix for target recognition. Whereas the target recognition by angular-diversity RCS techniques [12–14] requires  $181 \times 15 = 2715$  spatial directions (i.e., 181 azimuth angles and 15 elevation angles) in constructing the signal matrix for target recognition. Note that it is always difficult to build a spatial radar measurement in practical battlefield environments. The frequency diversity RCS technique of this study has indeed reduced the times of spatial radar measurement and is then an important contribution in target recognition. To enhance the discrimination, this study utilizes kernel scatter difference technique of pattern recognition. Numerical simulation shows that our target recognition scheme not only gives accurate identification but also significantly reduces the data dimension. The target recognition scheme in this study can also be applied to many other problems of radar engineering.

#### ACKNOWLEDGMENT

The authors would like to thank (1) the financial support from the Ministry of Science and Technology, Taiwan, under Grant MOST 108-2221-E-006-091, (2) the National Center for High Performance Computing, Taiwan, for computer time and facilities, and (3) Dr. Sheng-Chih Chan for his help in this study.

#### REFERENCES

1. Liu, S., R. Zhan, J. Zhang, and Z. Zhuang, “Radar automatic target recognition based on sequential vanishing component analysis,” *Progress In Electromagnetics Research*, Vol. 145, 241–250, 2014.



2. Osman, H., L. Pan, S. Blostein, and L. Gagnon, "Classification of ships in airborne SAR imagery using backpropagation neural networks," *Proceedings of the SPIE Radar Processing, Technology, and Applications II*, Vol. 3161, 126–136, San Diego, USA, September 24, 1997.
3. Zhou, J., Z. Shi, X. Cheng, and Q. Fu, "Automatic target recognition of SAR images based on global scattering center model," *IEEE Transactions on Geoscience and Remote Sensing*, Vol. 49, 3713–3729, 2011.
4. Martorella, M., E. Giusti, L. Demi, Z. Zhou, A. Cacciamano, F. Berizzi, and B. Bates, "Target recognition by means of polarimetric ISAR images," *IEEE Transactions on Aerospace and Electronic Systems*, Vol. 47, 225–239, 2011.
5. Musman, S., D. Kerr, and C. Bachmann, "Automatic recognition of ISAR ship image," *IEEE Transactions on Aerospace and Electronic Systems*, Vol. 32, 1392–1403, 1996.
6. Ruck, G. T., D. E. Barrick, W. D. Stuart, and C. K. Krichbaum, *Radar Cross Section Handbook*, Vol. 1, Plenum, New York, 1970.
7. Lee, S.-J., I.-S. Choi, B. Cho, E. J. Rothwell, and A. K. Temme, "Performance enhancement of target recognition using feature vector fusion of monostatic and bistatic radar," *Progress In Electromagnetics Research*, Vol. 144, 291–302, 2014.
8. Lee, K. C., "Polarization effects on bistatic microwave imaging of perfectly conducting cylinders," Master Thesis, National Taiwan University, Taipei, Taiwan, 1991.
9. Farhat, N. H., "Microwave diversity imaging and automated target identification based on models of neural networks," *Proceedings of the IEEE*, Vol. 77, 670–681, 1989.
10. Chi, C. and N. H. Farhat, "Frequency swept tomographic imaging of three-dimensional perfectly conducting objects," *IEEE Transactions on Antennas and Propagation*, Vol. 29, 312–319, 1981.
11. Farhat, N. H., T. Dzekov, and E. Ledet, "Computer simulation of frequency swept imaging," *Proceedings of the IEEE*, Vol. 64, 1453–1454, 1976.
12. Chan, S. C. and K. C. Lee, "Radar target identification of ships by kernel principal component analysis on RCS," *Journal of Electromagnetic Waves and Applications*, Vol. 26, 64–74, 2012.
13. Chan, S. C. and K. C. Lee, "Radar target recognition by MSD algorithms on angular diversity RCS," *IEEE Antennas and Wireless Propagation Letters*, Vol. 12, 937–940, 2013.
14. Chan, S. C. and K. C. Lee, "Angular-diversity target recognition by kernel scatter-difference based discriminant analysis on RCS," *International Journal of Applied Electromagnetics and Mechanics*, Vol. 42, 409–420, 2013.
15. Liu, Q. S., X. Tang, H. Q. Lu, and S. D. Ma, "Kernel scatter-difference based discriminant analysis for face recognition," *Proceedings of the International Conference on Pattern Recognition*, Vol. 2, 419–422, Cambridge, UK, August 26, 2004.
16. Liu, Q. S., X. Tang, H. Q. Lu, and S. D. Ma, "Face recognition using kernel scatter-difference based discriminant analysis," *IEEE Transactions on Neural Networks*, Vol. 17, 1081–1085, 2006.
17. Duda, R. O., P. E. Hart, and D. G. Stork, *Pattern Classification*, Wiley, New York, 2001.